Nuclear Science and Techniques (2023) 34:168
https://doi.org/10.1007/s41365-023-01301-4

Investigation of the ^{121}Sb(α,γ)^{125}I reaction cross-section calculations at astrophysical energies

M. Eroğlu[1,2] · C. Yalçın[1] · R. T. Güray[1]

Received: 23 March 2023 / Revised: 15 June 2023 / Accepted: 25 June 2023
© The Author(s), under exclusive licence to China Science Publishing & Media Ltd. (Science Press), Shanghai Institute of Applied Physics, the Chinese Academy of Sciences, Chinese Nuclear Society 2023

Abstract
Proton-rich nuclei are synthesized via photodisintegration and reverse reactions. To examine this mechanism and reproduce the observed p-nucleus abundances, it is crucial to know the reaction rates and thereby the reaction cross sections of many isotopes. Given that the number of experiments on the reactions in astrophysical energy regions is very rare, the reaction cross sections are determined by theoretical methods whose accuracy should be tested. In this study, given that ^{121}Sb is a stable seed isotope located in the region of medium-mass p-nuclei, we investigated the cross sections and reaction rates of the ^{121}Sb(α,γ)^{125}I reaction using the TALYS computer code with 432 different combinations of input parameters (OMP, LDM, and SFM). The optimal model combinations were determined using the threshold logic unit method. The theoretical reaction cross-sectional results were compared with the experimental results reported in the literature. The reaction rates were determined using the two input parameter sets most compatible with the measurements, and they were compared with the reaction rate databases: STARLIB and REACLIB.

Keywords Cross section · Astrophysical S-factor · Astrophysical reaction rate · p-process nucleosynthesis · Threshold logic unit method

1 Introduction

Most iron-heavy nuclei in nuclear charts are produced by neutron capture reactions in various astrophysical environments. Approximately 30 stable nuclei exist in the proton-rich region of the stability valley in the chart, which are referred to as *p* nuclei.-Specifically, *p*-nuclei are synthesized by a nuclear reaction mechanism termed as the astrophysical *p*-process [1]. The production of *p*-nuclei is initiated by the photodisintegration reactions of seed nuclei formed via neutron capture reactions [2]. As the neutron separation energy increases after sequential neutron emissions, the (γ,α) and (γ,p) reactions begin to compete with the (γ,n) reactions, and the *p*-process reaction path deviates toward the lower mass region [3, 4].

The (γ,α) and (α,γ) reactions are important due to the abundance of medium and heavy *p*-nuclei, where experimental studies are limited. Specifically, *p*-process nucleosynthesis has been modeled using an expanded nuclear reaction network, where information on the reaction rates of thousands of neutrons, protons, and α-induced reactions, as well as of their reverse reactions, is required [5, 6]. The corresponding astrophysical reaction rates obtained from the reaction cross sections are necessary inputs for the reaction network [7]. Unfortunately, experimental data on the charged particle-induced reactions of nuclei heavier than iron are rare. A limited number of proton capture reaction ([8–12] and cited in Ref. [13]) and α-capture reaction ([14–17] and cited in Ref. [18]) cross sections have been measured. Therefore, process studies rely mostly on theoretical cross sections from Hauser–Feshbach statistical models to estimate reaction rates. The overall reliability of Hauser–Feshbach predictions in *p*-process simulations has been discussed [19], and given that the variations in results can lead to significant changes in *p*-process abundance calculations, statistical models should be tested by comparing them with experimental results.

✉ R. T. Güray
tguray@kocaeli.edu.tr

[1] Department of Physics, Kocaeli University, Umuttepe, 41001 Kocaeli, Turkey

[2] Department of Electronics and Automation, Piri Reis University, 34940 Tuzla, Istanbul, Turkey

Published online: 14 November 2023

As ^{121}Sb is a stable seed isotope in the region of medium-mass p-nuclei, the investigation of ^{121}Sb is important for astrophysical reaction rate predictions and extend the experimental database required for an improved understanding of p-isotope production. Given the experimental difficulties in photodisintegration reactions, the reliability of statistical model predictions is limited to testing the reverse alpha capture reaction process. The (α,γ) reaction cross sections of this isotope were experimentally measured [18] to expand the experimental database and test the theoretical models. However, these measurements did not cover the astrophysical energy range (Gamow window). Therefore, a detailed theoretical study should be conducted to reasonably predict the cross sections of astrophysical energies. Hence, different models of optical potential, level density, and strength function should be considered. All these models affect the theoretical cross-sectional calculations, especially in the low-energy region, where the optical α+nucleus potential is likely to introduce the largest deviations in the charged particle reactions [20–23]. In this study, ^{121}Sb(α,γ)^{125}I reaction cross-sections and astrophysical S-factor values were calculated for 432 different combinations of eight optical potentials, six level densities, and nine strength function models and compared with the experimental results. The optimal model combinations were determined using threshold logic unit method [24]. The reaction rates were determined using the most compatible input parameter sets for the measurements. The obtained reaction rates were compared with those in existing reaction rate databases [25, 26]. This study can be applied not only in nuclear astrophysics but also in other fields where knowledge of reaction cross sections is required, such as medical physics and nuclear technology.

2 Method and calculation

2.1 Thermonuclear reaction rate

Thermonuclear reactions play important roles in the nucleosynthesis of these elements. The average reaction rate per pair of particles was derived from [27].

$$\langle \sigma v \rangle = \left(\frac{8}{\pi \mu} \right)^{1/2} \frac{1}{(kT)^{3/2}} \int_0^\infty \sigma(E) E \exp\left(-\frac{E}{kT} \right) \mathrm{d}E \tag{1}$$

where σ is the reaction cross section, E is the energy, T is the temperature, μ is the reduced mass, and k is the Boltzmann constant. Given that the cross section changes dramatically at low energies (astrophysical energy range), extrapolation of the experimental results to low energies is unreliable. The cross section can be given based on the astrophysical S-factor, $S(E)$, which smoothly changes with energy [27],

$$\sigma(E) = \frac{1}{E} \exp(-2\pi\eta) S(E) \tag{2}$$

where $S(E)$ includes all nuclear effects and η denotes the Sommerfeld parameter, which is given as follows:

$$\eta = \frac{Z_1 Z_2 e^2}{\hbar v}. \tag{3}$$

In this case, the reaction rate can be expressed as follows:

$$\langle \sigma v \rangle = \left(\frac{8}{\pi \mu} \right)^{1/2} \frac{1}{(kT)^{3/2}} \int_0^\infty S(E) \exp\left[-\frac{E}{kT} - \frac{b}{E^{1/2}} \right] \mathrm{d}E \tag{4}$$

where b denotes barrier penetration.

$$b = (2\mu)^{1/2} \pi e^2 Z_1 Z_2 / \hbar \tag{5}$$

Given that the S-factor changes more slowly in the astrophysical energy region, it would be better to investigate the model calculation of S-factors with a combination of input parameters that are most compatible with the experimental results.

2.2 Inputs for the model calculation

^{121}Sb(α,γ)^{125}I reaction cross sections were predicted using the TALYS 1.96 computer code [28] which uses Hauser–Feshbach statistical model calculations. Optical model potentials (OMP), level density models (LDM), and strength function models (SFM) play important roles in theoretical cross-sectional calculations. Detailed information on the models can be found in the relevant literature. To investigate the sensitivities of these parameters to the reaction cross sections, they are calculated for combinations of eight OMP, six LDM, and nine SFM, as listed in Tables 1, 2, and 3 .

OMP serve as a major input parameter in the calculation of the cross section in the astrophysical energy range. The OMP used in these calculations are denoted as OMP-1 through OMP-8. They consist of the normal alpha potential by Watanabe [29], the work of McFadden and Satchler [30], contributions from Demetriou et al. [31], Avrigeanu et al. [32]—which is the default selection of the code—along with the research of Nolte et al. [33] and another study by Avrigeanu et al. [34].

Three macroscopic and three phenomenological density models were used for the calculations. Phenomenological LDM include the constant temperature + Fermi gas model [35], back-shifted Fermi gas model [36, 37], and generalized superfluid model [38, 39], labeled as LDM-1 through LDM-3. Two macroscopic LDM were selected using the Skyrme force from Goriely's (LDM-4) [40] and Hilaire's (LDM-5) [41] tables. The third macroscopic

Table 1 Optical model potentials (OMP), which are available in the TALYS code. The default options for OMP is the Avrigeanu et al. (2014) (OMP-6)

Model no.	Optical model potential
OMP-1	Normal alpha potential [29]
OMP-2	McFadden and Satchler [30]
OMP-3	Demetriou et al. [31] (Table 1)
OMP-4	Demetriou et al. [31] (Table 2)
OMP-5	Demetriou et al. [31] (dispersive model)
OMP-6	Avrigeanu et al. [32]
OMP-7	Nolte et al. [33]
OMP-8	Avrigeanu et al. [34]

Table 2 Level density models (LDM), which are available in the TALYS code. The default options for LDM is constant temperature + Fermi gas model (LDM-1)

Model no.	Level density model
LDM-1	Constant temperature + Fermi gas model [35]
LDM-2	Back-shifted Fermi gas model [36, 37]
LDM-3	Generalized superfluid model [38, 39]
LDM-4	Microscopic level densities (Skyrme force) [40] from Goriely's tables
LDM-5	Microscopic level densities (Skyrme force) [41] from Hilaire's combinatorial tables
LDM-6	Microscopic LD (temp. dependent HFB, Gogny force) from Hilaire's combinatorial tables (2014) [42]

Table 3 Gamma-ray strength function models (SFM) which are available in the TALYS code. The default options for SFM is the Brink–Axel Lorentzian model (SFM-2)

Model no	Strength function model
SFM-1	Kopecky–Uhl generalized Lorentzian [43, 44]
SFM-2	Brink–Axel Lorentzian [45, 46]
SFM-3	Hartree–Fock BCS tables [47]
SFM-4	Hartree–Fock–Bogoliubov tables [48]
SFM-5	Goriely's hybrid model [49]
SFM-6	Goriely T-dependent HFB [50]
SFM-7	T-dependent RMF [51]
SFM-8	Gogny D1M HFB+QRPA [52]
SFM-9	Simplified Modified Lorentzian (SMLO) [53]

LDM used the Gogny force from Hilaire's combinatorial tables (LDM-6) [42]. The default option for the code was the constant temperature Fermi gas model (LDM-1) [35].

Nine different SFM are selected for the calculations, labeled SFM-1 through SFM-9, as listed in Table 3. The default option of the SFM is the Brink–Axel Lorentzian model (SFM-2) [45, 46].

In astrophysical environments, the reactions that occur within the astrophysical energy range are important. Consequently, calculations were performed in increments of 0.1 MeV, spanning from 6.00 to 14.5 MeV. This range encapsulates the astrophysical energy range known as the Gamow window, an overlapping region of the Maxwell–Boltzmann distribution and Coulomb barrier terms present in Eq. (4). Specifically, the Gamow window extends from 6.15 MeV to 8.68 MeV at a temperature of 3.0 GK for the ^{121}Sb(α,γ)^{125}I reaction [54].

2.3 Threshold logic unit method

The threshold logic unit (TLU) method was utilized to identify the most suitable input parameter sets from 432 combinations of eight OMP, six LDM, and nine SFM for the radiative alpha capture reaction of the ^{121}Sb isotope. The TLU method is fundamentally based on the concept of binary threshold functions. In this approach, each input is multiplied by a corresponding weight, and the sum of these weighted inputs is then compared with a predefined threshold value, as depicted in Eq. (7) [24]. If the sum surpasses the threshold, then the TLU generates an output of 1; otherwise, the output is 0.

In this study, the input values (X_i) were determined by comparing the TALYS results with experimental values within twice their uncertainties:

$$X_i = \begin{cases} 1 \text{ if } \quad \sigma_{Ei} - 2\Delta\sigma_{Ei} \le \sigma_{Ti} \le \sigma_{Ei} + 2\Delta\sigma_{Ei} \\ 0 \text{ otherwise} \end{cases} \tag{6}$$

where σ_{Ei} and σ_{Ti} denote the experimental and TALYS results, respectively, and $\Delta\sigma_{Ei}$ denotes the experimental uncertainty at energy i.

The obtained binary input values were compared with the threshold τ, and the best model combinations *BMC* were determined as follows:

$$\text{BMC} = \begin{cases} 1 \text{ if } \quad \sum_{i=1}^{n} (\theta_i X_i) \ge \tau \\ 0 \text{ otherwise} \end{cases} \tag{7}$$

In this context, the weight factors (θ_i) are designated as one, given that the weights of the cross sections remain uniform across all energy levels. The variable n denotes the number of energies at which the experiments were conducted. The threshold τ was chosen as the count of experimental energies where the TALYS outcomes aligned within twice their uncertainties with the experimental values. This implies that X_i is one; if not, X_i is zero. The ^{121}Sb(α,γ)^{125}I reaction cross sections were gauged at nine distinct energy levels;

consequently, n was set as nine, and the TLU method was employed for three threshold values, $\tau = 7$, 8, and 9. The reaction rates were computed from the TALYS results using the most fitting combinations of models that were congruous with the experimental values at all nine energy levels, i.e., a threshold of nine.

3 Results and discussion

The theoretical outcomes for the ^{121}Sb(α,γ)^{125}I reaction cross section and astrophysical S-factor were computed using 432 combinations of eight OMP, six LDM, and nine SFM. These results were then compared with the experimental values acquired at nine energy levels. The model parameters are denoted as $MP - ijk$, where i, j, and k represent $OMP - i$, $LDM - j$, and $SFM - k$, respectively, as listed in Tables 1, 2, and 3. In the study deploying the TLU method, 12 combinations are identified as compatible with the experimental outcomes at seven out of the twelve energies, as depicted in Fig. 1. Notably, a dramatic decrease in cross-sectional values predicted by the potential model labeled as 8 [34] is observed between 9 and 9.5 MeV. The significant depths illustrated in Figs. 1 and 2 could potentially be due to a numerical issue within the code.

The application of the TLU method identified only two combinations that aligned with the experimental results across all nine energy values. These two optimal matches (MP-338 and MP-432) were selected to calculate the reaction rates. The cross sections computed with the combinations of MP-338 and MP-432 produced consistent results, ranging between 0.76 and 1.20 times at all the experimental energy values.

The cross-sectional calculations conducted with identical OMP and LDM produced highly similar results across different SFM values, making them challenging to differentiate on the graphs. For instance, the cross-sectional results for MP-635 and MP-638 in Fig. 2 are very similar, although their differences become more pronounced in the astrophysical energy region.

The cross sections for the ^{123}Sb(α,n)^{126}I and ^{121}Sb(α,n)^{124}I reactions were also calculated using the top two combinations: MP-338 and MP-432. This was done to ascertain whether the results aligned acceptably with the measurements cited in the existing literature. The predicted values were found to be in agreement with the measurements of these reactions, as per Korkulu's research [18], which is demonstrated in Fig. 3.

Given the challenge in measuring the reaction cross section at lower energies and absence of experimental data within the Gamow window energy region, the theoretical results were compared with available experimental data at higher energies. For the combinations MP-338 and MP-432, which provided the closest theoretical outcomes to the experimental data, the reaction cross section and rate values are detailed in Tables 4 and 5, respectively. Furthermore, the average reaction rates for these two combinations

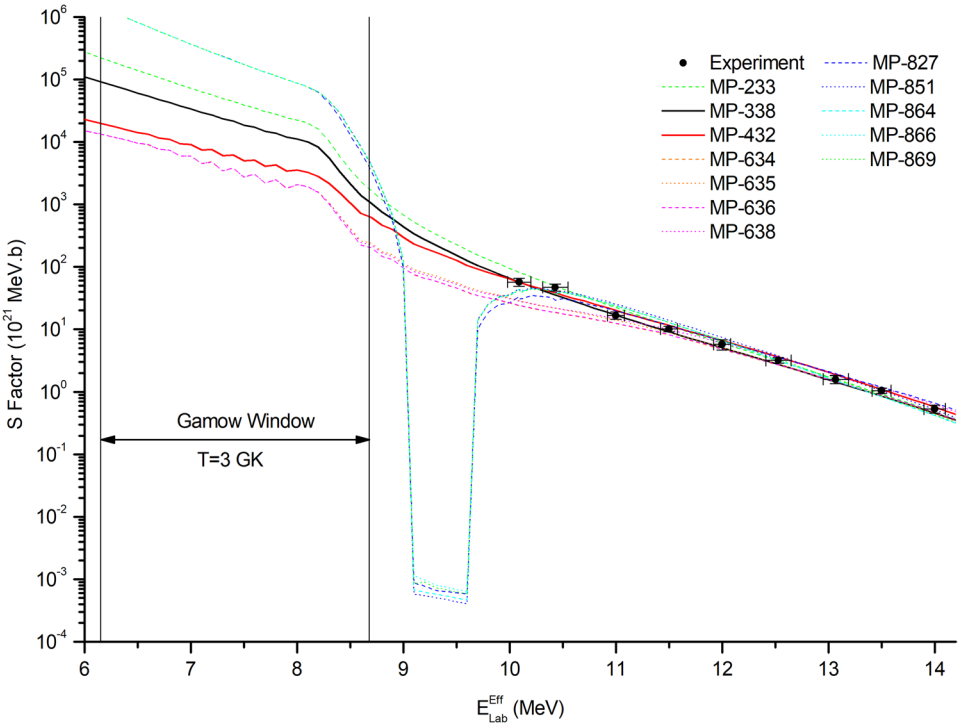

Fig. 1 (Color online) ^{121}Sb(α,γ)^{125}I S factors obtained by TALYS using the best 12 combinations selected. The first digit in the legend denotes the optical model number, the second digit denotes the level density model number, and the third digit denotes the strength function model number (Table 1, 2, and 3). The Gamow window at 3 GK is indicated on the plot

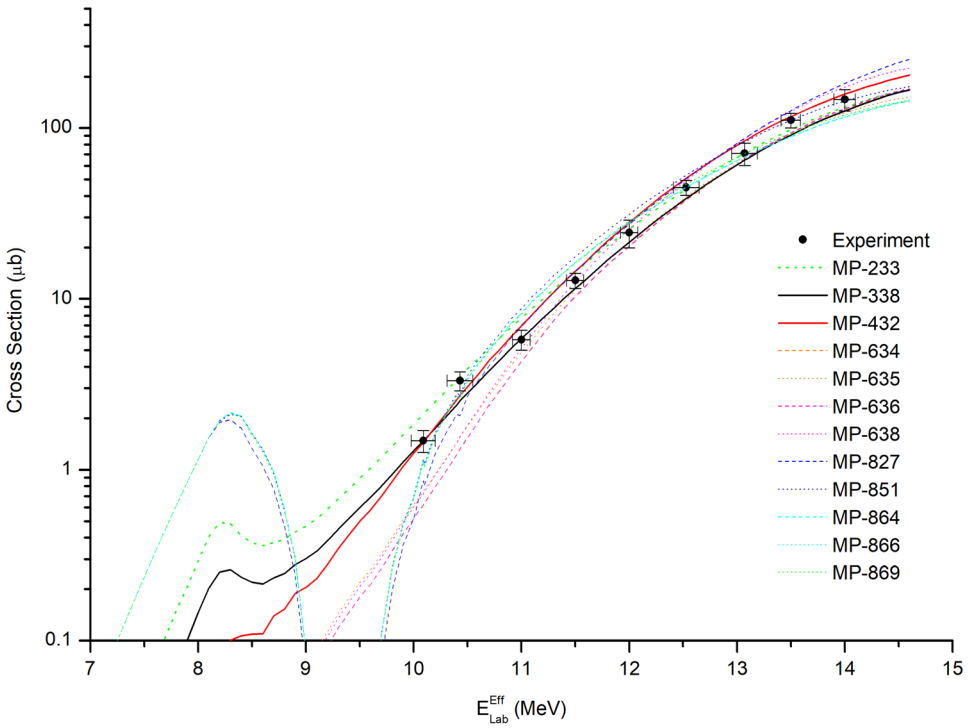

Fig. 2 (Color online) Cross sections of ^{121}Sb(α,γ)^{125}I obtained through TALYS using the top 12 selected combinations. The annotations align with those described in Fig. 1

are computed and graphed with respect to temperature, as depicted in Fig. 4.

4 Conclusion

The cross section and reaction rates of the ^{121}Sb(α,γ)^{125}I reaction, which plays a significant role in the p-process pathway of heavy nuclei responsible for the synthesis of proton-rich isotopes, were explored in this study. Although the radiative capture ^{121}Sb(α,γ)^{125}I reaction measurement does not offer complete information about the reverse photodisintegration reaction, it serves as a robust method to verify the reliability of the statistical model approach. Based on the resultant statistical model parameters, predictions of the cross section for the photofragmentation process can be directly derived within the scope of the Hauser–Feshbach model. This reaction was experimentally measured [18] to expand the available experimental database. However, as this experiment was conducted above the astrophysical energy range, the measured reaction cross sections must be extrapolated toward lower energies with high precision. The extrapolation of the determined astrophysical S-factor will yield more accurate results as it exhibits slower changes at lower energies when compared to the cross section.

A computer code utilizing the statistical Hauser–Feshbach approach was employed to identify theoretical results most compatible with the experimental data. The reaction

Table 4 Cross sections calculated with MP-338 and MP-432, their average values, and experimental values, for ^{121}Sb(α,γ)^{125}I reaction

$E_{Lab.}$ (MeV)	MP-338 μb	MP-432 μb	AVERAGE μb	Experiment[a] μb
6.00	3.10×10^{-5}	6.39×10^{-6}	1.87×10^{-5}	
6.50	3.96×10^{-4}	9.26×10^{-5}	2.45×10^{-4}	
7.00	3.68×10^{-3}	9.86×10^{-4}	2.33×10^{-3}	
7.50	2.50×10^{-2}	6.67×10^{-3}	1.58×10^{-2}	
8.00	1.46×10^{-1}	4.64×10^{-2}	9.61×10^{-2}	
8.50	2.20×10^{-1}	1.09×10^{-1}	1.65×10^{-1}	
9.00	3.02×10^{-1}	2.05×10^{-1}	2.53×10^{-1}	
9.50	6.00×10^{-1}	5.00×10^{-1}	5.50×10^{-1}	
10.0	1.29	1.25	1.27	
10.06	1.40	1.37	1.39	1.48 ± 0.22
10.41	2.45	2.63	2.54	3.32 ± 0.43
10.50	2.80	3.06	2.93	
10.97	5.64	6.69	6.17	5.77 ± 0.77
11.48	11.2	14.1	12.7	12.8 ± 1.3
11.98	20.9	27.3	24.1	24.4 ± 4.5
12.50	37.5	49.3	43.4	
12.51	37.9	49.8	43.9	44.9 ± 4.6
13.00	60.8	79.2	70.0	
13.05	63.6	82.8	73.2	70.9 ± 10.6
13.48	89.7	115	102	111 ± 11
13.99	125	157	141	147 ± 21
14.50	161	197	179	

[a]Ref. [18]

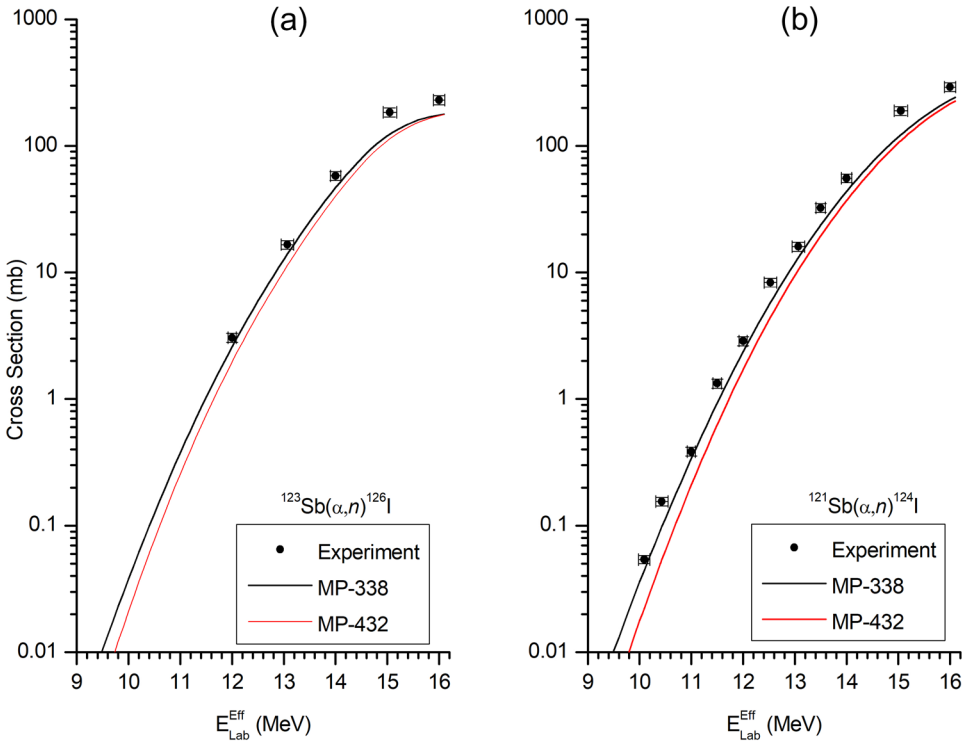

Fig. 3 (Color online) Cross sections of **a** ^{123}Sb(α,n)^{126}I and **b** ^{121}Sb(α,n)^{124}I obtained by TALYS using the best two combinations (MP-338 and MP-432)

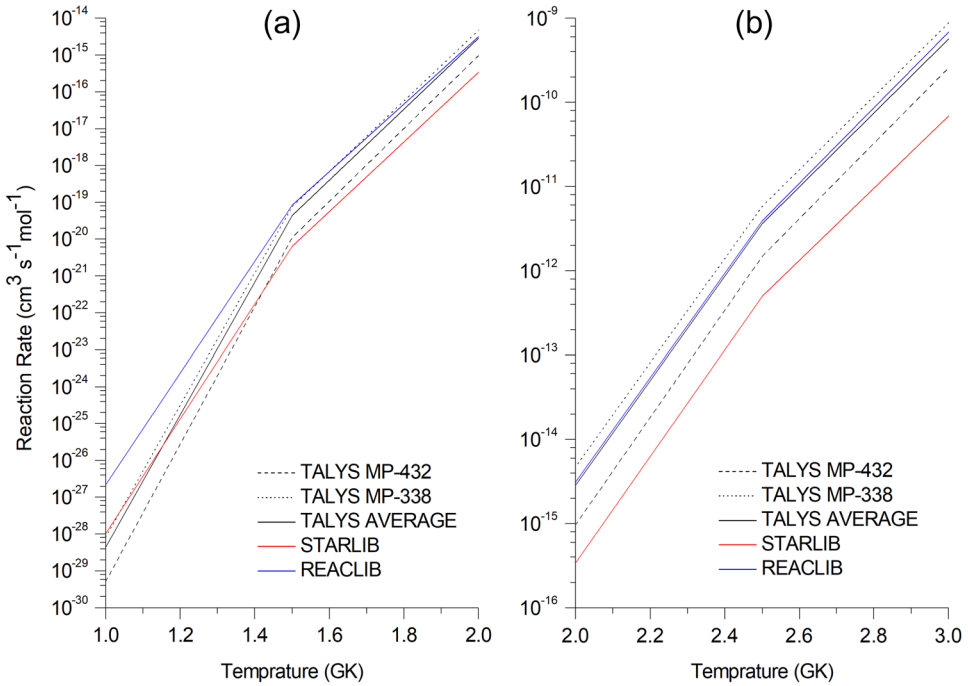

Fig. 4 (Color online) Reaction rates calculated with the cross sections using the most two compatible input parameter sets (MP-338 and MP-432) with the measurements. The average value of the two reaction rates for temperatures **a** between 1.0 and 2.0 GK and **b** between 2.0 and 3.0 GK

cross sections were computed using the TALYS code for 432 unique combinations of eight optical potentials, six level densities, and nine strength function models. The calculations that came closest to the experimental results were those obtained with the combinations of MP-338 and MP-432, determined via the TLU method. For nucleosynthesis networks, it is recommended to use the average reaction rate values that are most compatible with the experimental results.

The calculated average reaction rates were found to be compatible with STARLIB at lower temperatures (less than 1.4 GK) and with REACLIB at higher temperatures. Given

Table 5 Reaction rates calculated with the cross sections using the most two compatible input parameter sets (MP-338 and MP-432) with the measurements and their average values as suggested reaction rates for $^{121}Sb(\alpha,\gamma)^{125}I$

T (GK)	MP-338 cm^3/mol s	MP-432 cm^3/mol s	AVERAGE cm^3/mol s
1.0	8.44×10^{-29}	5.19×10^{-30}	4.48×10^{-29}
1.5	7.75×10^{-20}	1.11×10^{-20}	4.43×10^{-20}
2.0	4.76×10^{-15}	9.79×10^{-16}	2.87×10^{-15}
2.5	5.85×10^{-12}	1.49×10^{-12}	3.67×10^{-12}
3.0	8.79×10^{-10}	2.58×10^{-10}	5.69×10^{-10}
3.5	3.48×10^{-8}	1.16×10^{-8}	2.32×10^{-8}
4.0	5.58×10^{-7}	2.12×10^{-7}	3.85×10^{-7}
5.0	2.48×10^{-5}	1.31×10^{-5}	1.89×10^{-5}
6.0	2.63×10^{-4}	1.92×10^{-4}	2.27×10^{-4}
7.0	1.28×10^{-3}	1.14×10^{-3}	1.21×10^{-3}
8.0	4.06×10^{-3}	3.88×10^{-3}	3.97×10^{-3}
9.0	9.97×10^{-3}	9.57×10^{-3}	9.77×10^{-3}
10.0	1.99×10^{-2}	1.89×10^{-2}	1.94×10^{-2}

the substantial variations in the cross-sectional calculations made with different input parameter models, comparing the experimental results with the TALYS results, which only use the default parameters, may lead to misleading interpretations. To improve the accuracy of theoretical cross-sectional calculations, it is crucial to conduct additional experimentation at astrophysical energies to thoroughly test the existing models.

The TLU method can discern the most suitable models for each parameter to predict reaction cross sections that closely align with experimental data. Although recent studies in this field have predominantly utilized Chi-square tests, the TLU offers a different and simpler approach for future research endeavors.

Author contributions All authors contributed to the study conception and design. Material preparation, data collection, and analysis were performed by ME, CY, and RTG. The first draft of the manuscript was written by RTG, and all authors commented on previous versions of the manuscript. All authors read and approved the final manuscript.

References

1. S.E. Woosley, W.M. Howard, The p-processes in supernovae. Astrophys. J. Suppl. S. **36**, 285 (1978). https://doi.org/10.1086/190501
2. M. Arnould, S. Goriely, Astronuclear physics: a tale of the atomic nuclei in the skies. Prog. Part. Nucl. Phys. **112**, 103766 (2020). https://doi.org/10.1016/j.ppnp.2020.103766
3. R. Reifarth, C. Lederer, F. Käppeler, Neutron reactions in astrophysics. J. Phys. G Nucl. Partic. **41**, 053101 (2014). https://doi.org/10.1088/0954-3899/41/5/053101
4. T. Rauscher, N. Dauphas, I. Dillmann et al., Constraining the astrophysical origin of the p-nuclei through nuclear physics and meteoritic data. Rep. Prog. Phys. **76**, 066201 (2013). https://doi.org/10.1088/0034-4885/76/6/066201
5. T. Rauscher, F.K. Thielemann, Astrophysical reaction rates from statistical model calculations. Atom. Data Nucl. Data **75**, 1 (2000). https://doi.org/10.1006/adnd.2000.0834
6. T. Rauscher, F.K. Thielemann, Tables of nuclear cross sections and reaction rates: an addendum to the paper "astrophysical reaction rates from statistical model calculations. Atom. Data Nucl. Data **79**, 47 (2001). https://doi.org/10.1006/adnd.2001.0863
7. T. Rauscher, Branchings in the γ process path revisited. Phys. Rev. C **73**, 015804 (2006). https://doi.org/10.1103/PhysRevC.73.015804
8. Gy. Gyürky, Z. Halasz, G.G. Kiss et al., Measurement of the $^{91}Zr(p,\gamma)^{92m}$ Nb cross section motivated by type Ia supernova nucleosynthesis. J. Phys. G Nucl. Partic. **48**, 105202 (2021). https://doi.org/10.1088/1361-6471/ac2132
9. A. Palmisano-Kyle, A. Spyrou, P.A. DeYoung et al., Constraining the astrophysical p process: cross section measurement of the $^{84}Kr(p,\gamma)^{85}Rb$ reaction in inverse kinematics. Phys. Rev. C **105**, 065804 (2022). https://doi.org/10.1103/PhysRevC.105.065804
10. O.O. Gomez, A. Simon, O. Gorton et al., Measurements of proton capture in the A=100-110 mass region: constraints on the $^{111}In(\gamma, p)/(\gamma, n)$ branching point relevant to the γ process. Phys. Rev. C **102**, 055806 (2020). https://doi.org/10.1103/PhysRevC.102.055806
11. V. Foteinou, S. Harissopulos, M. Axiotis et al., Cross section measurements of proton capture reactions on Se isotopes relevant to the astrophysical p process. Phys. Rev. C **97**, 035806 (2018). https://doi.org/10.1103/PhysRevC.97.035806
12. S. Harissopulos, A. Spyrou, V. Foteinou et al., Systematic study of proton capture reactions in medium-mass nuclei relevant to the p process: the case of ^{103}Rh and $^{113,115}In$. Phys. Rev. C **93**, 025804 (2016). https://doi.org/10.1103/PhysRevC.93.025804
13. N. Özkan, R.T. Güray, C. Yalçın et al., Proton capture reaction cross section measurements on ^{162}Er as a probe of statistical model calculations. Phys. Rev. C **96**, 045805 (2017). https://doi.org/10.1103/PhysRevC.96.045805
14. J. Fallis, C. Akers, A.M. Laird et al., First measurement in the Gamow window of a reaction for the γ-process in inverse kinematics: $^{76}Se(\alpha,\gamma)^{80}Kr$. Phys. Lett. B **807**, 135575 (2020). https://doi.org/10.1016/j.physletb.2020.135575
15. T. Szuecs, P. Mohr, Gy. Gyürky et al., Cross section of α-induced reactions on ^{197}Au at sub-Coulomb energies. Phys. Rev. C **100**, 065803 (2019). https://doi.org/10.1103/PhysRevC.100.065803
16. G.G. Kiss, T. Szuecs, P. Mohr et al., α-induced reactions on ^{115}In: Cross section measurements and statistical model analysis. Phys. Rev. C **97**, 055803 (2018). https://doi.org/10.1103/PhysRevC.97.055803
17. T. Szuecs, G.G. Kiss, Gy. Gyürky et al., Cross section of α -induced reactions on iridium isotopes obtained from thick target yield measurement for the astrophysical γ process. Phys. Lett. B **776**, 396–401 (2018). https://doi.org/10.1016/j.physletb.2017.11.072
18. Z. Korkulu, N. Özkan, G.G. Kiss et al., Investigation of α-induced reactions on Sb isotopes relevant to the astrophysical γ process. Phys. Rev. C **97**, 045803 (2018). https://doi.org/10.1103/PhysRevC.97.045803
19. M. Arnould, S. Goriely, The p-process of stellar nucleosynthesis: astrophysics and nuclear physics status. Phys. Rep. **384**, 1 (2003). https://doi.org/10.1016/S0370-1573(03)00242-4
20. C. Yalçın, The cross section calculation of $^{112}Sn(\alpha,\gamma)^{116}Te$ reaction with different nuclear models at the astrophysical energy

range. Nucl. Sci. Tech. **28**, 113 (2017). https://doi.org/10.1007/s41365-017-0267-y
21. P. Mohr, Gy. Gyürky, Zs. Fülöp, Statistical model analysis of γ -induced reaction cross sections of ^{64}Zn at low energies. Phys. Rev. C **95**, 015807 (2017). https://doi.org/10.1103/PhysRevC.95.015807
22. R. Baldık, A. Yılmaz, A study on the excitation functions of ^{60,62}Ni(α, n), ^{60,61}Ni(α,2n), ^{58,64}Ni(α, p), ^{nat}Ni(α, x) reactions. Nucl. Sci. Tech. **29**, 156 (2018). https://doi.org/10.1007/s41365-018-0500-3
23. J.H. Luo, J.C. Liang, L. Jiang et al., Measurement of ^{134}Xe(n,2n)^{133m,g}Xe reaction cross sections in 14-MeV region with detailed uncertainty quantification. Nucl. Sci. Tech. **34**, 4 (2023). https://doi.org/10.1007/s41365-022-01158-z
24. R. Kruse, C. Borgelt, F. Klawonn et al., *Computational Intelligence* (Springer-Verlag, London, 2013), p.15
25. R.H. Cyburt, A.M. Amthor, R. Ferguson et al., The JINA REACLIB Database: Its Recent Updates and Impact on Type-i X-ray Bursts. Astrophys. J. Suppl. S. **189**, 240 (2010). https://doi.org/10.1088/0067-0049/189/1/240
26. A.L. Sallaska, C. Iliadis, A.E. Champange et al., STARLIB: a next-generation reaction-rate library for nuclear astrophysics. Astrophys. J. Suppl. S. **207**, 18 (2013). https://doi.org/10.1088/0067-0049/207/1/18
27. C.E. Rolfs, W.S. Rodney, *Cauldrons in the Cosmos* (The University of Chicago Press, Chicago, 1988), pp.156–159
28. A.J. Koning, S. Hilaire, M.C. Duijvestijn, in *Proceedings of the International Conference on Nuclear Data for Science and Technology*, ed. by O. Bersillon, F. Gunsing, E. Bauge, et al. Nice, April 2008. EDP Sciences, Vol. 1
29. S. Watanabe, High energy scattering of deuterons by complex nuclei. Nucl. Phys. **8**, 484 (1958). https://doi.org/10.1016/0029-5582(58)90180-9
30. L. McFadden, G.R. Satchler, Optical-model analysis of the scattering of 24.7 MeV alpha particles. Nucl. Phys. **84**, 177 (1966). https://doi.org/10.1016/0029-5582(66)90441-X
31. P. Demetriou, C. Grama, S. Goriely, Improved global α-optical model potentials at low energies. Nucl. Phys. A **707**, 253 (2002). https://doi.org/10.1016/S0375-9474(02)00756-X
32. V. Avrigeanu, M. Avrigeanu, C. Manailescu, Further explorations of the α-particle optical model potential at low energies for the mass range A≈45-209. Phys. Rev. C **90**, 044612 (2014). https://doi.org/10.1103/PhysRevC.90.044612
33. M. Nolte, H. Machner, J. Bojowald, Global optical potential for α particles with energies above 80 MeV. Phys. Rev. C **36**, 1312 (1987). https://doi.org/10.1103/PhysRevC.36.1312
34. V. Avrigeanu, P.E. Hodgson, M. Avrigeanu, Global optical potentials for emitted alpha particles. Phys. Rev. C **49**, 2136 (1994). https://doi.org/10.1103/PhysRevC.49.2136
35. A. Gilbert, A.G.W. Cameron, A composite nuclear-level density formula with shell corrections. Can. J. Phys. **43**, 1446 (1965). https://doi.org/10.1139/p65-139
36. W. Dilg, W. Schantl, H. Vonach et al., Level density parameters for the back-shifted fermi gas model in the mass range 40 < A < 250. Nucl. Phys. A **217**, 269 (1973). https://doi.org/10.1016/0375-9474(73)90196-6
37. P. Demetriou, S. Goriely, Microscopic nuclear level densities for practical applications. Nucl. Phys. A **695**, 95 (2001). https://doi.org/10.1016/S0375-9474(01)01095-8
38. A.V. Ignatyuk, K.K. Istekov, G.N. Smirenkin, Sov. J. Nucl. Phys. **29**, 450 (1979)
39. A.V. Ignatyuk, J.L. Weil, S. Raman et al., Density of discrete levels in 116Sn. Phys. Rev. C **47**, 1504 (1993). https://doi.org/10.1103/PhysRevC.47.1504
40. S. Goriely, S. Hilaire, A.J. Koning, Improved microscopic nuclear level densities within the Hartree-Fock-Bogoliubov plus combinatorial method. Phys. Rev. C **78**, 064307 (2008). https://doi.org/10.1103/PhysRevC.78.064307
41. S. Hilaire, S. Goriely, Global microscopic nuclear level densities within the HFB plus combinatorial method for practical applications. Nucl. Phys. A **779**, 63 (2006). https://doi.org/10.1016/j.nuclphysa.2006.08.014
42. S. Hilaire, M. Girod, S. Goriely et al., Temperature-dependent combinatorial level densities with the D1M Gogny force. Phys. Rev. C **86**, 064317 (2012). https://doi.org/10.1103/PhysRevC.86.064317
43. J. Kopecky, M. Uhl, Test of gamma-ray strength functions in nuclear reaction model calculations. Phys. Rev. C **41**, 1941 (1990). https://doi.org/10.1103/PhysRevC.41.1941
44. J. Kopecky, M. Uhl, R.E. Chrien, Radiative strength in the compound nucleus ^{157}Gd. Phys. Rev. C **47**, 312 (1993). https://doi.org/10.1103/PhysRevC.47.312
45. D.M. Brink, Individual particle and collective aspects of the nuclear photoeffect. Nucl. Phys. **4**, 215 (1957). https://doi.org/10.1016/0029-5582(87)90021-6
46. P. Axel, Electric dipole ground-state transition width strength function and 7-Mev photon interactions. Phys. Rev. **126**, 671 (1962). https://doi.org/10.1103/PhysRev.126.671
47. S. Goriely, E. Khan, Large-scale QRPA calculation of E1-strength and its impact on the neutron capture cross section. Nucl. Phys. A **706**, 217 (2002). https://doi.org/10.1016/S0375-9474(02)00860-6
48. S. Goriely, E. Khan, M. Samyn, Microscopic HFB + QRPA predictions of dipole strength for astrophysics applications. Nucl. Phys. A **739**, 331 (2004). https://doi.org/10.1016/j.nuclphysa.2004.04.105
49. S. Goriely, Radiative neutron captures by neutron-rich nuclei and the r-process nucleosynthesis. Phys. Lett. B **436**, 10 (1998). https://doi.org/10.1016/S0370-2693(98)00907-1
50. S. Hilaire, M. Girod, S. Goriely et al., Temperature-dependent combinatorial level densities with the D1M Gogny force. Phys. Rev. C **86**, 064317 (2012). https://doi.org/10.1103/PhysRevC.86.064317
51. D.P. Arteaga, P. Ring, Relativistic random-phase approximation in axial symmetry. Phys. Rev. C **77**, 034317 (2008). https://doi.org/10.1103/PhysRevC.77.034317
52. M. Martini, S. Hilaire, S. Goriely et al., Improved nuclear inputs for nuclear model codes based on the Gogny interaction. Nucl. Data Sheets **118**, 273 (2014). https://doi.org/10.1016/j.nds.2014.04.056
53. V. Plujko, O. Gorbachenko, K. Solodovnyk, Description of nuclear photoexcitation by Lorentzian expressions for electric dipole photon strength function. Eur. Phys. J. A **55**, 1–12 (2019). https://doi.org/10.1140/epja/i2019-12899-6
54. T. Rauscher, Relevant energy ranges for astrophysical reaction rates. Phys. Rev. C **81**, 045807 (2010). https://doi.org/10.1103/PhysRevC.81.045807

Springer Nature or its licensor (e.g. a society or other partner) holds exclusive rights to this article under a publishing agreement with the author(s) or other rightsholder(s); author self-archiving of the accepted manuscript version of this article is solely governed by the terms of such publishing agreement and applicable law.